Arabian Journal of Geosciences (2020) 13: 1267
https://doi.org/10.1007/s12517-020-06283-w

ORIGINAL PAPER

# Research on the bridge monitoring method of ground-based radar

Cheng Xing[1] · Peng Wang[2] · Wei Dong[3]

Received: 9 December 2019 / Accepted: 17 November 2020 / Published online: 25 November 2020


## Abstract

Bridge is an important infrastructure, and with the increase of bridge construction, the factors such as material aging and traffic congestion will affect the structural health of bridges. Therefore, the special attention should be paid to the regular deformation monitoring and health assessment of bridges. Due to the increasing monitoring requirements for large scale and span bridges, some new monitoring methods should be added as a complement to traditional monitoring methods such as precise leveling, total station, GNSS, terrestrial laser scanning, and so on. With the unique advantages of non-contact and real time, the microwave interferometry technology has become one of the means for deformation monitoring of bridges. The ground-based interferometric radar system has a high sampling rate in both the time and space domain, and it can be an effective complement to traditional methods. In this paper, the basic principle of ground-based interferometric radar system for dynamic deformation monitoring is briefly described. An improved projection method for computing the deflection with ground-based radar data is illustrated and is compared with the traditional projection method. A method for local relative deformation analysis of the bridge based on the characteristics of ground-based radar data is proposed. There are two parameters described for evaluating the local deformation of the bridge. Through the analysis of the deformation process of the bridge in a static load experiment, the feasibility of the method in the actual bridge structure safety monitoring is illustrated.

**Keywords** Ground-based interferometric radar · Deflection · Monitoring · Deformation analysis

## Introduction

Bridges, such as highway bridges, railway bridges, and high-speed railway bridges, play an important role in transportation and infrastructure construction. With the increase of bridge construction, the factors, such as material aging, fatigue of the structure, overload, traffic congestion, and natural/human hazards, will affect the structural health of bridges, and these factors may lead to bridge collapse and result in casualties and huge property losses. Therefore, regular deformation monitoring and health assessment of bridges are particularly important. Early detection of bridge defects can greatly save the maintenance cost of bridges, avoid the major losses caused by frequent overhaul of closed traffic, and minimize the losses caused by bridge accidents (Xu et al. 2007).

As the scale and span of bridges are increasing, the contents for bridge health monitoring are constantly improving (Huang et al. 2012). There are many traditional geodetic deformation monitoring methods, such as precise leveling, total station, GNSS, and terrestrial laser scanning, etc., each of which has advantages and disadvantages. The precision leveling method reflects the deflection deformation by regularly measuring the elevation of the monitoring points on the bridge, and the accuracy is high, but there are shortcomings such as time-consuming, interrupting the traffic, and poor real-time performance. The total station method measures the monitoring points in turn to obtain the deformation, and it can be used for the static and dynamic load test of bridges. But when it is applied to the dynamic deformation monitoring of long-span bridges, there will be problems such as environmental impacts and

Responsible Editor: Biswajeet Pradhan

✉ Cheng Xing
chxing@sgg.whu.edu.cn; 61626564@qq.com

Peng Wang
pwang@mail.usts.edu.cn

Wei Dong
dongwei_02@crfsdi.com

[1] School of Geodesy and Geomatics, Wuhan University, Wuhan 430079, China

[2] School of Environmental Science and Engineering, Suzhou University of Science and Technology, Suzhou 215009, China

[3] China Railway Siyuan Survey and Design Group Co., LTD, Wuhan 430063, China

simultaneous monitoring of each point. GNSS is also well applied in bridge monitoring with advantages of all-weather, high accuracy, real-time. But the spatial resolution is relatively lower because of the limit number of points selected on the bridge. 3D laser scanning technology can quickly obtain high-precision and high-density 3D point cloud with the characteristics of non-contact, automation, and large range. But the accuracy will decrease with the increase of the distance from the target. With the unique advantages of non-contact, real-time, and high spatial resolution, the microwave interferometry technology has gradually become one of the means for deformation monitoring of large and long-span bridges (Tarchi et al. 2003; Pieraccini et al. 2006; Pieraccini 2016; Xu et al. 2016; Guo et al. 2017), and it can be an effective complement to traditional methods. The ground-based interferometric radar system can accurately obtain the deformation along the line of sight in the target area. Compared with traditional geodetic deformation monitoring methods, the ground-based interferometric radar system does not need to have direct contact with the target area and has high sampling rates in both time and space (Huang et al. 2009). Accuracy comparisons have been made between ground-based microwave interferometry and the traditional transducers (such as accelerometers and seismometers), and it has been reported that ground-based microwave interferometry can achieve an accuracy of 0.1 mm (Pieraccini et al. 2008; Negulescu et al. 2013). This technology has a good application prospect in the deformation monitoring of linear targets such as bridges and high-rise buildings.

Many researchers have used the ground-based interferometric radar systems to conduct a large number of monitoring experiments and verified the feasibility of the system in practical projects. Qi et al. (2019) applied the IBIS-S (Image by Interferometric Survey–Structure, a real aperture radar system used for structural monitoring) to the bridge monitoring projects and compared the results of IBIS-S with the theoretical values to verify the correctness and reliability of IBIS-S. Diaferio et al. (2017) focused on an operational model analysis, which is extensively used as a tool for the model identification and the SHM (Structural Health Monitoring) of civil engineering constructions. The capability and the possible improvements of the ground-based radar interferometric experimental set-up for the periodic SHM of the spans of a railway viaduct are analyzed. Piniotis et al. (2016) conducted a dynamic test of a roadway, single-span, cable-stayed bridge for a sequence of static load and ambient vibration monitoring scenarios. A Ground-based Microwave Interferometer (GBMI) system was used for capturing the deck movements and cable vibrations. Rao et al. (2018) used the ground-based radar system to monitor the land subsidence for metro lines and obtained the displacements of the peripheral areas. Bernardini et al. (2007) conducted an IBIS-S accuracy test to verify that the monitoring accuracy of the radar system is better than 0.02 mm. Gentile and Bernardini (2008) completed the vibration test of the Capriaet Bridge. The results showed the consistency of the monitoring results of the ground-based radar system and the accelerometer. Diao (2010) applied the IBIS-S to CCTV building and bridge deformation monitoring and compared the monitoring results of IBIS with traditional surveying methods. The feasibility of this method in deformation monitoring and its advantages over traditional methods were analyzed. Liu (2009) used GPS RTK and microwave interferometry technology to monitor the displacements of some large and long-span bridges and evaluated the consistency of deflection obtained by these two methods. He et al. (2009) applied the interferometric radar system to the health monitoring of the bridges and compared the system with other surveying methods such as the accelerometers and total stations.

In this paper, we presented an improved projection method for calculating the deflection of the bridge with the ground-based radar data and made a comparison between the improved method and the traditional projection method. Furthermore, we proposed an analysis method with two parameters for evaluating the local relative deformation of the bridge. Finally, we designed a static load test for a bridge which is about to open to traffic for verifying the proposed methods, and the final results illustrate the correctness and feasibility of the proposed methods.

## Basic principle of deformation monitoring with ground-based interferometric radar

The ground-based interferometric radar systems mainly use the stepped-frequency continuous wave (SFCW) technology and interferometry technology (Diao and Huang 2009).

### Stepped frequency continuous wave

The stepped frequency continuous wave radar uses a frequency modulation system that uses $N$ consecutive frequency sequences (Zhang et al. 2009). This frequency sequence uniformly changes the frequency according to the step size of $\Delta f$ to send a sinusoidal signal sequence to a target and receiving the echo signal. The target's attribute and the detected target distance are obtained by synthesizing the pulse in time domain by propagating the baseband signal in the frequency domain (Park 2003). Figure 1 a shows the SFCW waveform in the time domain, Fig. 1b shows the SFCW waveform in the time-frequency domain, and Fig. 1c shows the synthesized pulse signal.

Where $N$ is the total number of consecutive pulses, $f_0$ is the initial frequency, $f_i$ ($i = 1, 2, \ldots, N - 1$) is the stepped frequency with the step size of $\Delta f$, PRI is the pulse repetition interval, which is the duration of a single frequency pulse, $B$ is the range bandwidth, $M$ is the number of IDFT, and $n_{\text{peak}}$ is the cell number corresponding to the main lobe's peak.

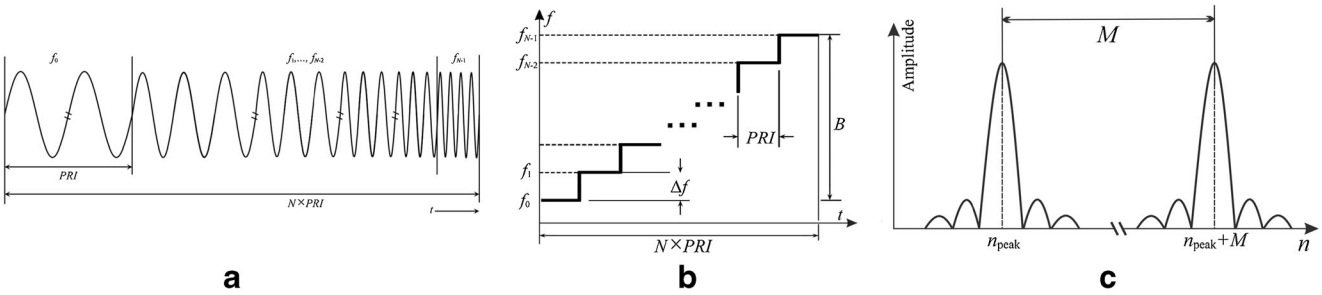


**Fig. 1** The diagram of SFCW waveform and synthetic pulse. **a** The SFCW waveform in the time domain. **b** The SFCW waveform in the time-frequency domain. **c** The synthesized pulse signal

The transmitted waveform of the SFCW radar can be expressed as

$$x_{\mathrm{i}}(\omega_{\mathrm{i}}, t) = A_{\mathrm{i}}\cos(\omega_{\mathrm{i}} t + \theta_{\mathrm{i}}) \tag{1}$$

where $\omega_{\mathrm{i}} = 2\pi(f_0 + i\Delta f)$, $i = 0, 1, 2, \ldots, N - 1$, $N$ is the total number of consecutive pulses, $f_0$ is the initial frequency, $\Delta f$ is the step size, $A_{\mathrm{i}}$ and $\theta_{\mathrm{i}}$ represent the amplitude and relative phase of the $i$th transmitted signal. The echo signal can be expressed as

$$r_{\mathrm{i}}(\omega_{\mathrm{i}}, t, \tau) = B_{\mathrm{i}}\cos[\omega_{\mathrm{i}}(t-\tau) + \theta_{\mathrm{i}}] \tag{2}$$

where $B_{\mathrm{i}}$ is the amplitude of the $i$th echo signal and $\tau$ is the round-trip time of the signal. The echo signal is down-converted into a baseband signal by a quadrature detector, and the normalized base-band in-phase ($I$) and quadrature ($Q$) signals after down-conversion are:

$$\begin{cases} I_{\mathrm{i}}(\omega_{\mathrm{i}}, \tau) = \cos(-\omega_{\mathrm{i}}\tau) = \cos\varphi_{\mathrm{i}} \\ Q_{\mathrm{i}}(\omega_{\mathrm{i}}, \tau) = \sin(-\omega_{\mathrm{i}}\tau) = -\sin\varphi_{\mathrm{i}} \end{cases} \tag{3}$$

The analog $I/Q$ signals are resampled to digital $I/Q$ signals by the $A/D$ converter. The target distance can be calculated from the phase ($\varphi = \omega_{\mathrm{i}}\tau$) of the $I/Q$ signal. In order to obtain the round-trip propagation time, a Fourier transform is required. The decoded signal is obtained by the digital $I/Q$ signals in complex vector form:

$$C_{\mathrm{i}} = I_{\mathrm{i}} + jQ_{\mathrm{i}} = \exp(-j\varphi_{\mathrm{i}}) \tag{4}$$

where $j$ is the imaginary unit.

The synthesized time domain response is obtained by using IDFT:

$$y_{\mathrm{n}} = \frac{1}{M}\sum_{i=0}^{M-1} C_{\mathrm{i}}\exp\left(\frac{j2\pi ni}{M}\right) \tag{5}$$

where $0 \le n \le M - 1$, $M$ is the sampling number of IDFT, i is the index of the complex vector $C$. The amplitude of the synthesized pulse is as follows:

$$|y_{\mathrm{n}}| = \left|\frac{\sin(aN/2)}{\sin(a/2)}\right|, a = \left(n - \frac{2M\Delta fR}{c}\right)\frac{2\pi}{M} \tag{6}$$

where $0 \le n \le M - 1$, $M$ is the sampling number of IDFT, $N$ is the total number of frequency steps, $\Delta f$ is the frequency step, and $R$ is the target distance. The synthesized pulse signal is shown in Fig. 1c. The synthesized pulse signal reaches the peak when $n = n_{\mathrm{peak}} + lM$, $a = \pm 2l\pi$, $l$ is an integer, and $l = 0, 1, 2, 3, \ldots$

The range resolution of the radar is determined by the bandwidth of the transmitted signal (Paulose 1994):

$$\Delta R = c/(2N\Delta f) = c/(2B) \tag{7}$$

where $\Delta R$ is the range resolution, $c$ is the light speed, $N$ is the total number of frequency steps, $\Delta f$ is the step size, and $B$ is the range bandwidth.

### Interferometry

The radar continuously monitors the target area, extracts the deformation phase by interference calculation between neighboring sampling signals, and calculates the displacements. The relationship between the line of sight (LOS) displacement ($\Delta_{\mathrm{los}}$) and the displacement phase ($\Delta\varphi$) is

$$\Delta_{\mathrm{los}} = -(\lambda/4\pi)\Delta\varphi \tag{8}$$

where $\lambda$ is the wavelength of the signal.

The ground-based interferometric radar system can generally achieve sub-millimeter-level monitoring accuracy. The accuracy can be better than 0.1 mm with a good field of view in the 500 m range and stable weather conditions (Pieraccini et al. 2004; Gentile and Bernardini 2009).

## Data processing methods

### Computation of deflection with radar data

#### The traditional method

Deflection is the displacement perpendicular to the bridge axis, whereas the result we obtain from the radar is the displacement along the LOS. Therefore, we need to make a projection to compute the deflection. The most general projection

method is to consider the LOS displacement as a component of the deflection and compute the deflection by the angle between the LOS and the horizontal direction (Gikas and Daskalakis 2011). The diagram of traditional method is shown in Fig. 2, the angle between the LOS and the horizontal direction is $\alpha$, and the deflection ($\Delta_v$) can be expressed as Equation (9). The projection result of this method can be used when the LOS displacement is smaller, but it will not be accurate enough when the LOS displacement becomes larger. The comparisons are shown in Table 1.

Where $R$ is the radar position, $A$ is a target point in the $i$th range bin (Rbin $i$, $i$th resolution unit along the line of sight) on the bridge, $L$ is the distance between the radar and point A, $H$ is the height from the radar to the bridge, $\Delta_v$ is the deflection, $\Delta_{los}$ is the deformation along LOS, $\alpha$ is the angle between the LOS and the horizontal direction, and $\alpha$ is also the angle between the vertical direction and the direction perpendicular to LOS.

$$\Delta_v = \Delta_{los}/\sin\alpha = \Delta_{los} \times (L/H) \tag{9}$$

Where in the right triangle AOB, $\sin\alpha = H/L$.

### An improved method

Point $A_0$ in range bin $i$ on the bridge is shown in Fig. 3; when the bridge is deformed, $A_0$ moves to $A_1$. The distance between $R$ and $A_0$ is $L_0$, the distance between $R$ and $A_1$ is $L_1$, and the displacement along LOS can be expressed as $\Delta_{los} = L_0 - L_1$.

Where $R$ is the radar position, $A_0$ is a target point in the $i$th range bin on the bridge, $A_1$ is the deformed position of $A_0$, $L$ and $L_1$ are the distance from the radar to point $A$ and $A_1$, respectively, $H$ is the height from the radar to the bridge, $\Delta_v$ is the deflection, $\Delta_{los}$ is the deformation along LOS, $\alpha$ is the angle between the LOS and the horizontal direction, and $\alpha$ is also the angle between the vertical direction and the direction perpendicular to LOS.

If the height between the bridge and the radar is $H$, the deflection ($\Delta_v$) can be expressed as

$$(L_0 - \Delta_{los})^2 - (H - \Delta_v)^2 = L_0^2 - H^2 \tag{10}$$

**Table 1** The comparison of the traditional and improved projection method. Where $H$ is the height from the radar to the bridge, $L_0$ is the distance between $R$ and $A_0$ (the initial position), $\Delta_{los}$ is the deformation along LOS, $\Delta_v$ is the deflection computed by the traditional method and $\Delta_v$' is by the improved method, and $\Delta$ is the difference between $\Delta$ and $\Delta_v$

| No. | $L_0$/m | $H$/m | $\Delta_{los}$/m | $\Delta_v$/mm | $\Delta'_v$/mm | $\Delta = \Delta_v - \Delta'_v$/mm |
|---|---|---|---|---|---|---|
| 1 | 300.000 | 30.000 | 0.005 | 50.04 | 50.00 | 0.04 |
| 2 | | | 0.010 | 100.17 | 100.00 | 0.17 |
| 3 | | | 0.020 | 200.66 | 200.00 | 0.66 |
| 4 | | | 0.030 | 301.50 | 300.00 | 1.50 |
| 5 | | | 0.040 | 402.68 | 400.00 | 2.68 |
| 6 | | | 0.050 | 504.20 | 500.00 | 4.20 |
| 7 | | | 0.060 | 606.06 | 600.00 | 6.06 |
| 8 | | | 0.070 | 708.28 | 700.00 | 8.28 |
| 9 | | | 0.080 | 810.85 | 800.00 | 10.85 |

If we suppose $L_0$ = 300 m, $H$ = 35 m, the accumulative displacement is $\Delta_{los}$ = 80 mm, the result of deflection computed with Equation (10) is $\Delta_v$ = 692.5 mm. If we use the traditional method, the result will be $\Delta_v$ = 685.7 mm. There is an obvious difference of 6.8 mm.

Table 1 shows a comparison list between the traditional and improved method, $\Delta_v$ is the deflection computed by Equation (10), and $\Delta'_v$ is the deflection computed by Equation (9). We can see that when the LOS displacement ($\Delta_{los}$) is smaller, the differences between the two methods are not very obvious and can be negligible. But when $\Delta_{los}$ becomes lager, the differences increase. Therefore, whether the improved method should be used depends on the accuracy of the measurements. For example, in the case of Table 1, if we want to obtain mm level monitoring results, the improved method should be used when the LOS displacement is larger than 0.02 m.

## Local deformation analysis for the bridge

The ground-based radar only captures the deformation of discrete points, but the spatial correlation between these discrete

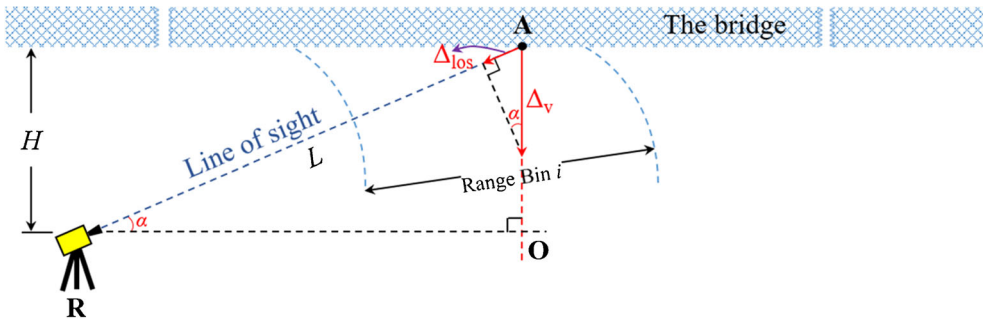


**Fig. 2** The diagram of traditional projection method for computing deflection

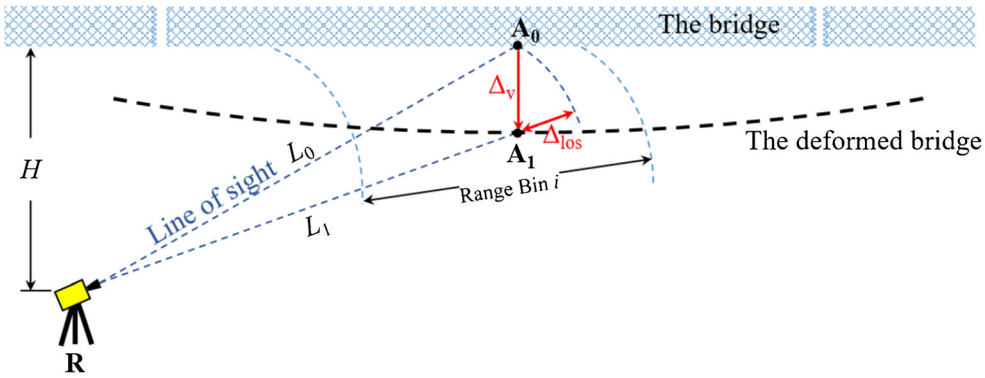


**Fig. 3** The diagram of improved method for computing deflection

points is not considered (Liu 2009; Rödelsperger et al. 2010). For linear structures such as bridges and high-rise buildings, the overall and local deformations have strong spatial correlation. The ground-based radar system has a high sampling rate in both time and space domain, the deflection and vibration characteristics of each range bin can be analyzed, and we can also analyze the correlation of local deformation using the deformation data of each range bin acquired at the same time. In this paper, we describe a relative deformation analysis method for the bridge.

A selected local structure unit $S$ is shown in Fig. 4, the length of this unit is $D$. Point $m$ represents the range bin in the middle of the selected unit, and there are also some other range bins such as $n$, $p$, $q$, and so on in this unit. From time $t_1$ to $t_2$, the deformation directions of point $m$ and point $n$ are the same but with different values, and neither the deformation direction nor values of point $m$ and point $p$ are the same. We can define two local relative variables, $\mu_{\mathrm{mn}}^{t_1}{}_{t_2}$ (deformation density) and $v_{\mathrm{mn}}^{t_1}{}_{t_2}$ (deformation speed), and these parameters can be expressed as Equation (11).

$$\begin{cases} \mu_{\mathrm{mn}}^{t_1 t_2} = \dfrac{|\Delta_{\mathrm{m}}^{t_1 t_2} - \Delta_{\mathrm{n}}^{t_1 t_2}|}{D_{\mathrm{mn}}} \\ v_{\mathrm{mn}}^{t_1 t_2} = \dfrac{|\Delta_{\mathrm{m}}^{t_1 t_2} - \Delta_{\mathrm{n}}^{t_1 t_2}|}{\Delta t} \end{cases} \tag{11}$$

where m represents the range bin in the middle of the selected unit, n represents other range bins in the selected unit, $\Delta_{\mathrm{m}}^{t_1}{}_{t_2}$ is the deformation from time $t_1$ to $t_2$, $D_{\mathrm{mn}}$ is the distance between points m and n, and $\Delta t = t_2 - t_1$. The weighted average of $\mu$ and $v$ in the selected unit can be expressed as

$$\begin{cases} \mu = \dfrac{\sum\limits_{\mathrm{n}\in S}\left(\dfrac{\mu_{\mathrm{mn}}^{t_1 t_2}}{D_{\mathrm{mn}}}\right)}{\sum\limits_{\mathrm{n}\in S}\dfrac{1}{D_{\mathrm{mn}}}} \\ v = \dfrac{\sum\limits_{\mathrm{n}\in S}\left(\dfrac{v_{\mathrm{mn}}^{t_1 t_2}}{D_{\mathrm{mn}}}\right)}{\sum\limits_{\mathrm{n}\in S}\dfrac{1}{D_{\mathrm{mn}}}} \end{cases} \tag{12}$$

where m represents the range bin in the middle of the selected unit, n represents other range bins in the selected unit, $S$ is the selected unit, $D_{\mathrm{mn}}$ is the distance between m and n, $\Delta_{\mathrm{mn}}^{t_1}{}_{t_2}$ is the deformation between m and n from time $t_1$ to $t_2$.

From Equation (12), we can see that $\mu$ reflects the relative deformation of each range bin in the selected unit to the center point m from time $t_1$ to $t_2$, and $v$ depends on the value we choose for $\Delta t$, it reflects the severity of the deformation of the bridge during the monitoring period.

We can use the above equations to calculate the relative deformation density and speed for each range bin to the reference point (the point represents the range bin in the middle of the selected unit). With these values, when we focus on the

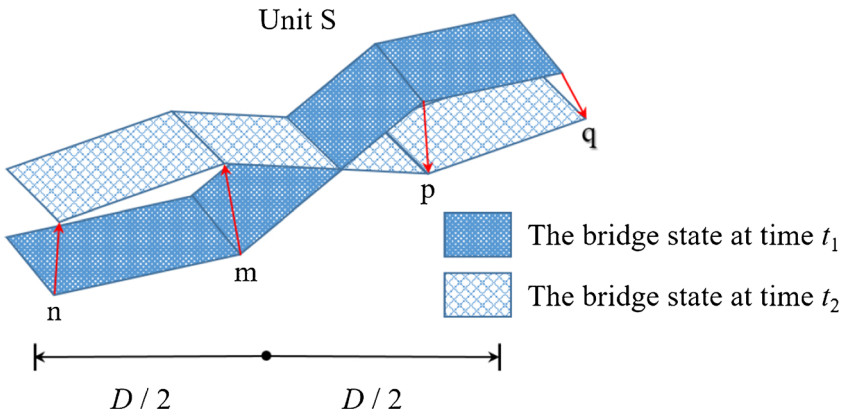


**Fig. 4** The relative deformation of the local area on the bridge

**Table 2** The parameters of IBIS-S

| Item | | Parameters |
|---|---|---|
| Antenna | Gain | 20 dBi |
| | Polarization type | VV |
| Signal | Frequency channel/wavelength | Ku/17.4 mm |
| | Bandwidth | 300 M (1.705~1.735 GHz) |
| | Frequency step | 57.703 kHz |
| Range resolution | | 0.75 m |
| Maximum monitoring distance | | 650 m |
| Duration | | 4500 s |
| Sampling rate | | 20 Hz |

points with large differences in the same direction of deformation and opposite direction of deformation, we can find out whether the local position of the bridge has an abnormal deformation or there is a tendency for abnormal deformation.

## Experiments

The ground-based radar system we used in the experiment is the IBIS-S (Image by Interferometric Survey-Structure), which is developed by IDS and University of Florence. The continuous micro-deformation monitoring with high accuracy can be provided by this system, and the accuracy can be better than 0.1 mm in case of stable weather conditions (Pieraccini et al. 2008; Pieraccini et al. 2004; Gentile and Bernardini 2009; Negulescu et al. 2013; Xu et al. 2016). The interferometric technique is applied in this system, and the covered targets can be monitored day and night.

The system parameters in the experiment are listed in Table 2. The monitoring target is a bridge on the Yangtze River in Wuhan, China, which was about to open to traffic, and the experiment was a static load test at midnight. Figures 5 and 6 show the monitoring diagram and the monitoring scene. The length of the monitored bridge span is about 620 m, and the height between the radar and the bridge is about 30 m. The furthest monitoring distance was set at 650 m, and the sampling rate was about 20 Hz.

**Fig. 6** The monitoring scene

There were three stages in the static load test: (1) 16 fully loaded trucks drove to the middle of the bridge; (2) another 16 fully loaded trucks drove to the middle of the bridge; and (3) all the trucks drove off the bridge. The experiment lasted about 4500 s. We use db4 wavelet (Chui 1992) and Birgé-Massart strategy to pre-process the radar signal for noise reduction (Yi et al. 2006).

Since the universal beams are evenly arranged at the bottom of the bridge (shown in Fig. 6), the reflection conditions are very well. The signal intensity is very high, and the signal peak distribution is relatively uniform (the SNR map is shown in Fig. 7). Due to the large number of peaks, only feature points are marked with red circles. It is obvious that the radar signals gradually decrease as the distance increases.

The target points are filtered with an empirical threshold of 44 dB (shown in Fig. 8a). Figure 8 b shows the positions of the selected points on the bridge.

Taking the selected target points as the analysis objects, the deformation projection is performed according to the method in "An improved method", and the vertical deformation trends of several important positions and key moments are plotted in Fig. 9. Figure 9 shows that the first batch of fully loaded trucks entered the bridge at the time of 1400 s, the second batch entered at the time of 2600 s, all the trucks began to leave at

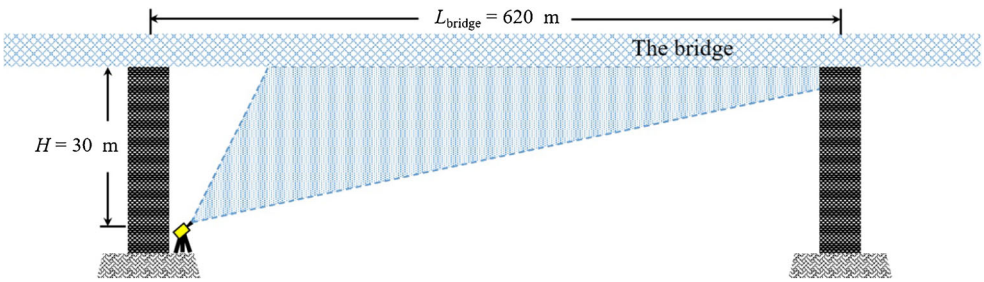


**Fig. 5** The monitoring diagram

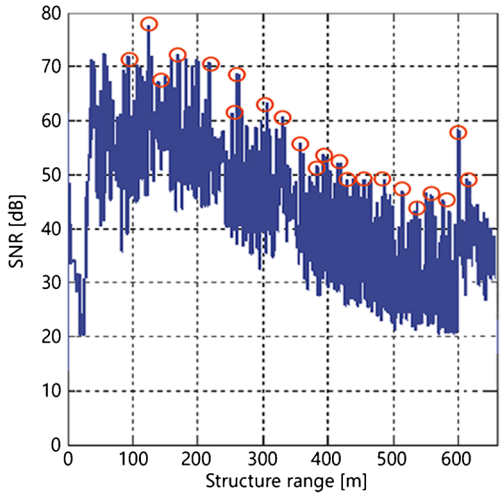


**Fig. 7** SNR map of targets

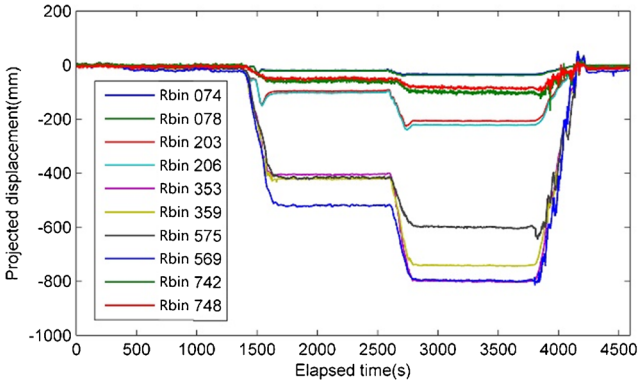


**Fig. 9** The deflection curves

3800 s, and the bridge restored to its initial state at about 4150 s. It was a gradual stable process when the trucks entered and left the bridge. The deformation reached the maximum at the time of 2800 s and at the position of 260 m.

## Discussion

According to "An improved method", the LOS displacements in the experiment are very large, so the deflections should be computed by the improved projection method with Equation (10), and these results are shown in Fig. 9.

According to the collected radar data, for each selected range bin, $\mu$ and $v$ can be calculated according to Equation (10), we set $\Delta t = 1$ s, $D = 20$ m, the initial time is 1000 s, and select 5 representative results listed in Table 3. Then, we can analyze the correlation of the deformation in local space in the static load test.

Based on the calculated data in Fig. 9 and Table 3, the $\mu$ and $v$ values of the five initial times of the respective bridge positions can be compared. The results show that the values of $\mu$ and $v$ in the unloaded state and the load balance state are small, and the state of the bridge is relatively stable. The $\mu$ and $v$ values in the process of loading and unloading are obviously becoming larger, which reflects the sensitivity of $\mu$ and $v$ to the deformation.

The small displacement of the central position within the selected unit does not always mean the deformation is not severe. For example, in Unit No. 2, the displacement at the time of 2600 s is larger than that at 1400 s, but the $\mu$ and $v$ are smaller, which means that the relative deformation within Rbin 203 at 1400 s is larger, and the relative deformation speed is faster. This result indicates that the relative deformation at 1400 s is more severe. Another example is between Unit No. 2 and Unit No. 4, at the time of 2800 s, the displacement of Rbin 203 is larger than that of Rbin 575, but the $\mu$ and $v$ are smaller, which means that the relative deformation around Rbin 575 is more severe.

From Table 3, we can see that the relative deformation density ($\mu$) reflects the intensity of spatial deformation between adjacent points, and the relative deformation speed ($v$) reflects the severity of the deformation between adjacent points in the time domain. The values of $\mu$ and $\nu$ show different behaviors in different selected units, and the reason for this phenomenon is that the values of $\mu$ and $\nu$ in different units are influenced by the displacements of selected range bins and different time intervals. With the results of the experiment,

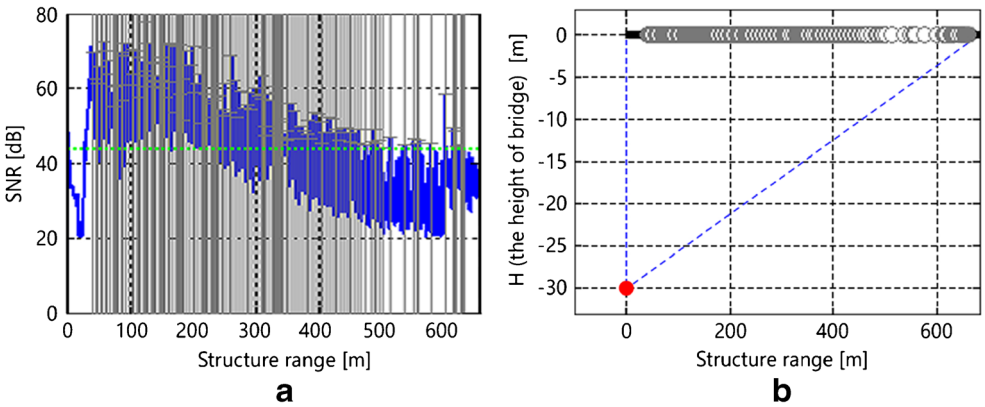


**Fig. 8** Target point selection. **a** The SNR threshold. **b** Target point positions on the bridge

**Table 3** Local relative deformation analysis

| Unit No. | Central Rbin No. | Neighboring Rbin No. | Time (s) | Central Rbin displacement (mm) | $\mu$ (mm/m) | $v$ (mm/s) |
|---|---|---|---|---|---|---|
| 1 | 78 | 70, 74, 82, 87 | 1400 | − 2.56 | 0.06 | 0.81 |
| | | | 1600 | − 16.31 | 0.42 | 3.76 |
| | | | 2600 | − 20.18 | 0.63 | 2.09 |
| | | | 2800 | − 28.90 | 0.77 | 2.32 |
| | | | 3800 | − 29.14 | 0.78 | 1.50 |
| | | | 4250 | − 1.05 | 0.02 | 0.03 |
| 2 | 203 | 192, 199, 206, 209, 211 | 1400 | − 15.88 | 4.56 | 37.80 |
| | | | 1600 | − 59.19 | 1.32 | 7.87 |
| | | | 2600 | − 66.01 | 0.97 | 2.10 |
| | | | 2800 | − 135.24 | 1.18 | 4.19 |
| | | | 3800 | − 135.21 | 1.12 | 3.91 |
| | | | 4250 | − 3.29 | 0.06 | 0.07 |
| 3 | 353 | 359, 365 | 1400 | − 16.73 | 0.17 | 3.18 |
| | | | 1600 | − 301.88 | 2.80 | 33.31 |
| | | | 2600 | − 329.00 | 2.76 | 10.08 |
| | | | 2800 | − 583.36 | 9.88 | 33.48 |
| | | | 3800 | − 583.31 | 10.00 | 21.75 |
| | | | 4250 | − 14.38 | 0.11 | 0.26 |
| 4 | 575 | 569, 587 | 1400 | − 13.48 | 1.46 | 17.94 |
| | | | 1600 | − 80.93 | 1.57 | 18.33 |
| | | | 2600 | − 88.47 | 1.41 | 6.44 |
| | | | 2800 | − 128.71 | 1.41 | 4.53 |
| | | | 3800 | − 134.56 | 2.58 | 4.60 |
| | | | 4250 | − 16.44 | 1.45 | 2.19 |
| 5 | 742 | 736, 748, 754 | 1400 | − 5.89 | 0.43 | 6.01 |
| | | | 1600 | − 47.35 | 1.69 | 13.29 |
| | | | 2600 | − 49.54 | 1.88 | 6.11 |
| | | | 2800 | − 74.01 | 2.33 | 6.13 |
| | | | 3800 | − 79.32 | 1.87 | 3.14 |
| | | | 4250 | − 9.22 | 1.05 | 1.62 |

**Table 4** The comparison of $\mu$ and $v$ with different number of points selected

| Unit No. | Central Rbin No. | Neighboring Rbin No. | Time (s) | $\mu$ (mm/m) | $v$ (mm/s) |
|---|---|---|---|---|---|
| 2 | 203 | 192, 199, 206, 209, 211 | 1400 | 4.56 | 37.80 |
| | | | 1600 | 1.32 | 7.87 |
| | | | 2600 | 0.97 | 2.10 |
| | | | 2800 | 1.18 | 4.19 |
| | | | 3800 | 3.12 | 3.91 |
| | | | 4250 | 0.06 | 0.07 |
| 2 | 203 | 199, 206, 209 | 1400 | 5.07 | 35.38 |
| | | | 1600 | 1.39 | 6.78 |
| | | | 2600 | 1.04 | 1.89 |
| | | | 2800 | 1.42 | 4.04 |
| | | | 3800 | 3.36 | 3.50 |
| | | | 4250 | 0.06 | 0.06 |

we can see that besides the accumulated displacements, the values of $\mu$ and $\nu$ can also effectively reflect the severity of deformation between the local range bins on the bridge, and more reliably evaluate the local deformation of the bridge.

From Equation (11) and Equation (12), we can see that the values of $\mu$ and $\nu$ are influenced by the choice and the number of the measurement points, but only the points close to the center have main influence on the values, the points further away from the center have less impact on the results. We take Unit No. 2 for example to compare the values of $\mu$ and $\nu$ with different number of measurement points, and the results are shown in Table 4. Table 4 shows that different numbers of measurement points have less influence on the values of $\mu$ and $\nu$, and the results are mainly affected by the measurement points close to the center. In the actual data processing, we can select 1~3 points in the neighborhood of the center.

When we analyze the results of the static and dynamic load test or repeated monitoring, the deformation parameters under the same conditions can be statistically analyzed. However, no matter the accumulated displacements or the parameters $\mu$ and $\nu$ mentioned above, the warning thresholds for bridge structural health need to be set not only with the geometric monitoring results but also in combination with the monitoring results of multiple professional fields. Therefore, the threshold of these two parameters ($\mu$ and $\nu$) needs to be discussed in conjunction with further experimental results in more professional fields.

## Conclusions

In this paper, we presented an improved projection method for computing the deflection of the bridge, with which we can get a more accurate deflection. We also proposed a local relative deformation analysis method for the characteristics of bridge deformation, which can reliably reflect the severity of local deformation of the bridge and evaluate the overall safety status and risk areas of the bridge.

In the dynamic health monitoring for bridges, if the parameters of the local relative deformation analysis can be calculated in real time, combined with the monitoring results such as displacement time series analysis and spectrum analysis, it will be much better for the comprehensive assessment of the bridge structural health and the emergency response of the bridge disaster. However, the health status of the bridge needs to be comprehensively evaluated in combination with the monitoring results of various fields. In the further researches, more and more extensive experiments are needed to study various factors which may affect the health of the bridge.

**Authors' contributions** Conceptualization, Cheng Xing and Peng Wang; methodology, Cheng Xing; software, Cheng Xing and Peng Wang.; formal analysis, Peng Wang; data curation, Wei Dong; writing—original draft preparation, Cheng Xing; writing—review and editing, Peng Wang and Wei Dong.

**Funding** The work was supported by the CRSRI Open Research Program (Program SN:CKWV2017518/KY), the Project Based Personnel Exchange Program with China Scholarship Council and German Academic Exchange Service of 2018 (No. [2019]12039), the National Natural Science Foundation of China (Grant No. 41801381), and the Hubei Provincial Natural Science Foundation (NO. 2017CFB654).

## Compliance with ethical standards

**Conflict of interest** The authors declare that they have no conflict of interest.

## References

Bernardini G, De Pasquale G, Bicci A, Marra M, Coppi F, Ricci P, Pieraccini M (2007) Microwave interferometer for ambient vibration measurements on civil engineering structures: 1. Principles of the radar technique and laboratory tests. Proceedings of the International Conference on Experimental Vibration Analysis of Civil Engineering Structures, Porto

Chui CK (1992) Wavelets: a tutorial in theory and applications. Academic Press Professional, Inc., San Diego

Diaferio M, Fraddosio A, Piccion MD, Castellano A, Mangialardi L, Soria L (2017) Some issues in the structural health monitoring of a railway viaduct by ground based radar interferometry. IEEE Workshop on Environmental, Energy, and Structural Monitoring Systems (EESMS), Milan, Italy

Diao J (2010) Application of microwave interferometer in dynamic monitoring of a high-rising building. J Vibration Shock 29:177–179, 261. https://doi.org/10.13465/j.cnki.jvs.2010.11.042

Diao J, Huang S (2009) Application of ground-based InSAR building deformation monitoring. Bull Surv Mapp 9:45–47

Gentile C, Bernardini G (2008) Radar-based measurement of deflections on bridges and large structures: radar techniques and static tests. RILEM Symposium on Site Assessment of Concrete Masonry and Timber Structures: 507 - 517. https://doi.org/10.1080/19648189.2010.9693238

Gentile C, Bernardini G (2009) An interferometric radar for non-contact measurement of deflections on civil engineering structures: laboratory and full-scale tests. Struct Infrastruct Eng 6:521–534. https://doi.org/10.1080/15732470903068557

Gikas V, Daskalakis S (2011) Radar-based measurements of the oscillation parameters of large civil engineering structures. Joint International Symposium on Deformation Monitoring, Hong Kong, China

Guo P, Zhang W, Chen L, Zhou K, Wang C (2017) A novel FMCW GB-SAR based bridge deformation measurement campaign. Bull Surv Mapp 6:94–97. https://doi.org/10.13474/j.cnki.11-2246.2017.0198

He N, Guan B, Qi Y, He B (2009) Application of movement and surveying radar in the bridge health monitoring. Modern Transp Technol 6:31–33

Huang S, Yang B, You X (2009) Applications of GPS dynamic geometric deformation monitoring system to Sutong Bridge. Geomatices Inform Sci Wuhan Univ 34:1072–1075. https://doi.org/10.13203/j.whugis2009.09.015

Huang S, Luo L, He C (2012) Comparative test analysis for determining bridge deflection by using ground-based SAR and GPS. Geomatices Inform Sci Wuhan Univ 37:1173–1176. https://doi.org/10.13203/j.whugis2012.10.015

Liu D (2009) Comparative analysis of GPS measurement and microwave interference measurement applied to measurement of bridge dynamic deflection. Bridge Constr 472:81–84

Negulescu C, Luzi G, Crosetto M, Raucoules D, Roullé A, Monfort D, Pujades L, Colas B, Dewez T (2013) Comparison of seismometer and radar measurements for the modal identification of civil engineering structures. Eng Struct 51:10–22. https://doi.org/10.1016/j.engstruct.2013.01.005

Park J (2003) Development of microwave and millimeter-wave integrated-circuit stepped-frequency radar sensors for surface and subsurface profiling. Dissertation, Texas A&M University, USA

Paulose A (1994) High radar range resolution with the step frequency waveform. Dissertation, Naval Post-graduate School, USA

Pieraccini M (2016) Extensive measurement campaign using interferometric radar. J Perform Constr Facil 31:04016113. https://doi.org/10.1061/(ASCE)CF.1943-5509.0000987

Pieraccini M, Fratini M, Parrini F, Atzeni C (2004) High-speed CW step-frequency coherent radar for dynamic monitoring of civil engineering structures. Electron Lett 40:907–908. https://doi.org/10.1049/el:20040549

Pieraccini M, Luzi G, Mecatti D, Noferini L, Atzeni C (2006) Ground-based SAR for short and long term monitoring of unstable slopes. Proceedings of the 3rd European Radar Conference, Manchester

Pieraccini M, Fratini M, Parrini F, Atzeni C, Partoli G (2008) Interferometric radar vs. accelerometer for dynamic monitoring of large structures: an experimental comparison. NDT E Int 41:258–264. https://doi.org/10.1016/j.ndteint.2007.11.002

Piniotis G, Gikas V, Mpimis A, Perakis H (2016) Deck and cable dynamic testing of a single-span bridge using radar interferometry and videometry measurements. J Appl Geodesy 10:87–94. https://doi.org/10.1515/jag-2015-0030

Qi B, Yue S, Song Y (2019) Application of GBInSAR technology in bridge deformation monitoring. Geospatial Inform 15:97–98. https://doi.org/10.3969/j.issn.1672-4623.2017.07.029

Rao X, Cao C, Teng H, Jiang L, Zhou Q, Huang R, Gao B (2018) Application of foundation InSAR technology in deformation monitoring of transit. Modern Urban Transit 7:25–28

Rödelsperger S, Läufer G, Gerstenecker C, Becker M (2010) Monitoring of displacements with ground-based microwave interferometry: IBIS-S and IBIS-L. J Appl Geodesy 4:41–54. https://doi.org/10.1515/jag.2010.005

Tarchi D, Casagli N, Fanti R, Leva D, Luzi G, Pasuto A, Pieraccini M, Silvano S (2003) Landslide monitoring by using ground-based SAR interferometry: an example of application to the Tessina Landslide in Italy. Eng Geol 68:15–30. https://doi.org/10.1016/S0013-7952(02)00196-5

Xu H, Guo G, Pu H, Yuan M (2007) Causes and lessons of bridge accidents in China in recent years. China Safety Sci J 17:90–95. https://doi.org/10.16265/j.cnki.issn1003-3033.2007.11.018

Xu J, Liao H, Han D, Xing C (2016) New methods for deflection measurement of bridge with large span. Bull Surv Mapp 1:91–94. https://doi.org/10.13474/j.cnki.11-2246.2016.0023

Yi T, Li H, Yi X, Wang G (2006) On GPS observation errors with ANC principles and wavelet denoise method. Geomatics Inform Sci Wuhan Univ 31:995–998. https://doi.org/10.13203/j.whugis2006.11.014

Zhang L, Li N, Hu C, Li P (2009) Radar target scattering characteristics test and imaging diagnosis. China Aerospace Publishing House, Beijing